Article

Development of Novel AlSi10Mg Based Nanocomposites: Microstructure, Thermal and Mechanical Properties

Seyed Kiomars Moheimani [1], Mehran Dadkhah [2],* and **Abdollah Saboori [2]**

[1] Department of Materials Engineering, Najafabad Branch, Azad University, Najafabad 8514143131, Iran; kiomars.moheimani@gmail.com

[2] Department of Applied Science and Technology, Politecnico di Torino, Corso Duca Degli Abruzzi 24, 10129 Torino, Italy; abdollah.saboori@polito.it

* Correspondence: mehran.dadkhah@polito.it; Tel.: +39-391-426-1099

check for updates

Abstract: Al matrix nanocomposites are interestingly employed in the automotive, military, aerospace and electronics packaging industries. In this study, Graphene Nanoplatelets (GNPs) reinforced AlSi10Mg nanocomposites were produced via powder metallurgy. The effect of GNPs content on density, microstructure and mechanical characteristics of the AlSi10Mg/GNPs nanocomposites was investigated systematically. To this aim, AlSi10Mg/GNPs nanocomposites reinforced with 0.5, 1.0 and 2.0 wt.% of GNPs were produced by wet mixing method following by hot compaction at 600 °C. To evaluate the effect of GNPs on mechanical properties of the as-fabricated nanocomposite, Vickers hardness and tensile properties of composites analyzed at room temperature. According to the results, it was found that the fabrication of AlSi10Mg/GNPs nanocomposites is faced with several challenges such as agglomeration and non-uniform dispersion of GNPs that should be addressed to achieve the desirable thermal and mechanical properties. For instance, surprisingly, it is revealed that the mechanical and thermal properties of nanocomposites were deteriorated in the presence of a high quantity of GNPs (>1.0 wt.%), which can be attributed to the GNPs agglomeration and accordingly introduction of internal porosity in the nanocomposite. The relatively low fraction of GNPs can uniformly be dispersed in the matrix and improve the performance of the nanocomposite.

Keywords: metal matrix nanocomposite; Al alloys; graphene; mechanical properties; microstructure

1. Introduction

Graphene is composed of a single atomic layer of sp^2 hybridized carbon atoms, which attracted more attention as an interesting reinforcement in metal matrix nanocomposites (MMNCs) owing to the particular properties such as electrical [1–3] and mechanical properties [4,5], and it's fascinating thermal properties [4,6]. The few-layer graphene (FLG) with high specific surface area is well-known as a desirable reinforcement in MMNCs, so that results in the production of MMNCs with excellent mechanical properties [7]. Moreover, low density of Graphene Nanoplatelets (GNPs) causes the increase of its applications in weight-reduction of MMNCs, ceramics or polymers [8–10]. Regarding the application of GNPs in the production of Ceramic Matrix Nanocomposite (CMNCc), Wang et al. indicated that in the presence of 2.0 wt.% GNPs, the fracture toughness of Al_2O_3 can be improved by up to 53% [10]. In another work, the fracture toughness of monolithic Si_3N_4 was enhanced up to 136% by the addition of 1.5 vol.% GNPs [11].

Nevertheless, according to recent research, the production of GNP reinforced MMNCs has been attracting worldwide attention due to their excellent characteristics. Thus far, among the MMNCs reinforced by GNPs, Mg–GNPs [12,13], Cu–GNPs [14–16] and Al–GNPs [17,18] nanocomposites are the

most interesting nanocomposites that have been developed. For instance, in 2014, Rashad et al. found that the better GNPs dispersion within aluminum achieved by the liquid state mixing of GNPs in Al powder [19]. Their results showed that through the uniform distribution of GNPs within the metallic matrix, it would be possible to effectively improve the final properties of composites. In another work, Wang et al. produced Al-Multilayered Graphene (Al–MLG) through the combination of conventional powder metallurgy and hot extrusion [20]. Saboori et al. investigated the effect of GNPs on the microstructure and mechanical properties of Al/GNPs nanocomposites produced via powder metallurgy and hot rolling methods [21]. They have shown that a uniform dispersion of GNPs within the matrix can be achieved only at low GNPs contents, and after a specific quantity, the GNPs agglomerates start to form and deteriorate the final mechanical properties of the composite. In another work, it was found that by increasing the GNPs content, the compressibility and sinterability of Al composites decrease markedly, which resulted in the higher porosity content in the final composites [22]. Rashad et al. studied the mechanical performance of magnesium matrix composites reinforced by GNPs, and their results indicated that a homogeneous dispersion of GNPs can result in an increment in microhardness, tensile strength and fracture strain of those composites [23]. The Cu-GNPs nanocomposite is another interesting nanocomposite that was developed by Saboori et al. [16]. In fact, they produced Cu-GNPs composites via classical powder metallurgy followed by hot isostatic pressing (HIP). It was found that the relative density of Cu and Cu composites increases by using the HIP process. In fact, by using HIP as post-process, it would be possible to eliminate the residual porosities and consequently improve the mechanical properties and thermal conductivity of the composites. Bartolucci et al. fabricated Al/GNPs composites via HIP and extrusion [24]. Their findings indicate that GNPs are prone to forming Al_4C_3 during the process that accordingly deteriorates the hardness and tensile strength of Al composites. Saboori et al. fabricated Cu-GNPs nanocomposites using a wet mixing method followed by conventional powder metallurgy [3]. In their work, ball milling and wet mixing as two different mixing methods to disperse the GNPs within the copper powder were considered and compared. Their microstructural evaluations showed that ball milling is not a proper method to disperse the GNPs within the Cu matrix, whereas the wet mixing method has great potential to be employed as a dispersion method.

Nevertheless, to date, there are few studies that have investigated the association between the microstructure, mechanical and thermal properties of AlSi10Mg alloy and the GNPs content. Therefore, this research aimed to explore the effect of GNPs on the microstructure, mechanical and thermal properties of AlSi10Mg alloy. Thus, different weight percentages of GNPs (0, 0.5, 1.0 and 2.0 wt.%) were added to AlSi10Mg by using the wet mixing method followed by hot compaction at 600 °C. Thereafter, thermal conductivity and mechanical characteristics of AlSi10Mg-GNPs nanocomposites were evaluated, as well as the microstructure.

2. Materials and Methods

In this study, graphene nanoplatelets with 99% purity, 100 nm thickness and 25 μm width together with a spherical gas-atomized AlSi10Mg powder with 35 μm average size were used as starting materials. The chemical composition of the starting AlSi10Mg powder is shown in Table 1. Based on the datasheets, the densities of GNPs and AlSi10Mg powders were 2.2 and 2.67 g/cm^3, respectively.

Table 1. Chemical composition (wt.%) of the AlSi10Mg alloy.

Al	Si	Fe	Cu	Mn	Mg	Ni	Zn	Pb	Sn	Ti
Balance	9–11	≤0.56	≤0.05	≤0.43	≤0.2–0.45	≤0.05	≤0.11	≤0.05	≤0.05	≤0.15

The nanocomposite powder mixture is prepared via a wet mixing method proposed by Rashad et al. [25]. In this method, at first, GNPs were dispersed in ethanol through ultrasonication for 45 min. Simultaneously, AlSi10Mg powders were separately dispersed via mechanical agitation in ethanol. Then, to achieve the final mixture of AlSi10Mg/GNPs, after ultrasonication, GNPs were inserted dropwise into the Al powder slurry. Afterwards, to improve the homogeneity, the mixtures

were mechanically agitated for 60 min using a mechanical agitator. Subsequently, the powder mixture was filtered and dried at 80 °C for 6 h. The consolidation of nanocomposites was performed via hot compaction at 600 °C. For this reason, the final nanocomposite powder mixtures were consolidated in stainless steel die with 15 mm diameter under 30 kN for 25 min at 600 °C. To have a reference sample, pure AlSi10Mg samples are considered and produced in the same way nanocomposites. The microstructural characterization of as-received materials and consolidated AlSi10Mg-GNPs nanocomposite were carried out using a Merlin-Zeiss FESEM (field emission scanning electron microscope) (Merlin-Zeiss, München, Germany), operating at 15 kV and a light optical microscope. Grain size evaluation was carried out via the intercept method on three OM images, and the average is reported as the grain size.

In addition, the structure of as-received GNPs was evaluated by using a Raman spectroscopy analysis. Raman spectra of GNPs were analyzed using a Renishaw In Via Reflex micro-Raman spectrometer (Renishaw plc, Wotton-under-Edge, UK) equipped with a cooled charge-coupled device camera. Before irradiating the samples, the laser beam was focused using a 50× objective lens. tensile properties of the hot consolidated samples were evaluated via a testing machine (MTS Alliance RF/150) at room temperature using a crosshead displacement rate of 1 mm/min. For the statistical point of view, three samples for each composition were prepared parallel to the compaction direction with a gauge length of 20 mm and a diameter of 6 mm. Moreover, Young's modulus of the specimens was measured by a nondestructive test based on the impulse excitation vibration method. Thermal conductivity of samples was assessed by a laser flash method using a FLASHLINETM apparatus (Anter Corporation, Pittsburgh, PA, USA). In order to increase the laser absorption during the thermal conductivity tests, both sides of the samples were coated with a thin layer of graphite.

3. Results and Discussion

3.1. Microstructure Characterization

The morphology of AlSi10Mg powder is demonstrated in the FESEM image (Figure 1a). As can be seen, the particles are mainly spherical and contain some satellites and agglomerates of fine particles. Figure 1b depicts that a thin layer of the molten alloy was covered the AlSi10Mg powder and also the starting powder includes some internal porosities that can adversely affect the mechanical characteristics and final density of nanocomposites. The FESEM micrograph of as-received GNPs is shown in Figure 1c.
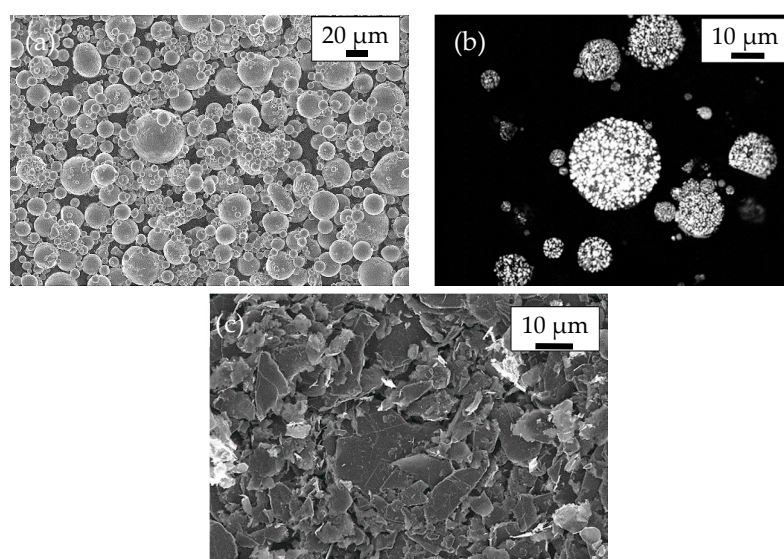

Figure 1. (**a**) Scanning electron microscope (SEM) micrograph of as-received AlSi10Mg power, (**b**) Light Optical Microscopy (LOM) image of the cross-section of AlSi10Mg powder, (**c**) SEM micrograph of graphene nanoplatelets.

Based on the Raman spectra, there are three distinct bands at 1331, 1580 and 2680 cm^{-1}, which are related to the D band (disorder related), G band (graphite related), and 2D band (second-order), respectively. By an intensity ratio of the 2D band to G band it was confirmed that as-received graphene is not a single-layer. In addition, the presence of a small number of defects in as-received graphene was confirmed by the ratio of G band over D band, which is equal to 0.12. However, evaluation of composite powder mixture after the mixing indicates that the ratio of G band over D band remains almost unchanged (0.122) that confirms that through the wet mixing method it would be possible to mix the GNPs with the metallic powder without introducing any defect in its structure (Figure 2).
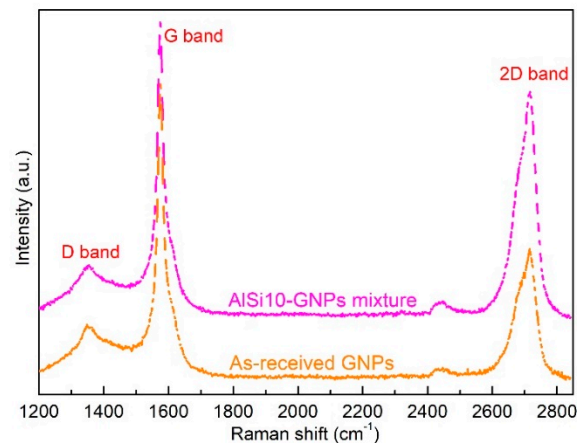

Figure 2. Raman spectra of as-received graphene nanoplatelets and AlSi10Mg-GNPs nanocomposite powder after mixing.

The porosity evaluation of samples was performed via image analysis method on five images per sample, and the average values are reported as the average porosity content of samples.

This porosity analysis indicated that the porosity content of samples was fairly limited and is in the range of 0.04–0.25% for the AlSi10Mg–GNPs nanocomposites. Figure 3a–d demonstrates representative microstructure of AlSi10Mg–x wt.%GNPs (x = 0, 0.5, 1.0, 2.0) nanocomposites after hot consolidation at 600 °C. As can be seen, the microstructure of AlSi10Mg (Figure 3a) consists of α-Al solid solution as the white matrix and dispersed eutectic Si particles that are detectable like a dark phase. In addition, it was found that despite a homogeneous dispersion of GNPs (the black phase at the grain boundaries) within the AlSi10Mg matrix after the hot consolidation, by increasing the GNPs content the number of graphene agglomerates increased markedly (Figure 3b–d). Moreover, grain size evaluation via the intercept method showed that the grain size of nanocomposites decreases from 23 ± 3.5 μm for AlSi10Mg to 15 ± 1.7 μm for AlSi10Mg–2%GNPs. It means the introduction of GNPs also resulted in slight grain refinement in the nanocomposite materials.

As is revealed in Figure 3a,b, a rather homogeneous dispersion of GNPs particles in the AlSi10Mg matrix achieved that cause to the increment in mechanical features due to the grain reinforcement and Orowan strengthening mechanisms. However, in the case of AlSi10Mg-GNPs nanocomposites with high GNPs contents, some large agglomerates of GNPs can be seen at the grain boundaries (Figure 3c,d), which occur as a result of Pi–Pi interaction between graphene nanoplatelets. Therefore, according to the findings of the previous works, it can be expected that this agglomerate formation adversely affects the mechanical performance of nanocomposite [26].

Figure 4a–d is the Optical micrographs of AlSi10Mg–xGNPs (x = 0, 0.5, 1.0, 2.0 wt.%). These images were achieved in the cross-section parallel to the hot consolidation direction. As shown in Figure 4a, the microstructure of AlSi10Mg alloys is the same as its microstructure in the perpendicular direction that brings the isotropic properties in this material. The microstructure of Alsi10Mg-GNPs nanocomposites shows that the GNPs had a preferred orientation during the consolidation and the majority of nanoplatelets are oriented in the perpendicular direction of compaction. This preferred

orientation of GNPs, which is also revealed in the literature [27], leads to anisotropic behavior of materials. This anisotropic behavior could be due to the significant difference between the in-plane and out-of-plane properties of graphene and its preferred orientation during the compaction. According to inherent properties of GNPs, the out of plane strength (weak physical bonding between the layers) of GNPs is much less than its in-plane strength (strong chemical bonding between the atoms of the same layer).
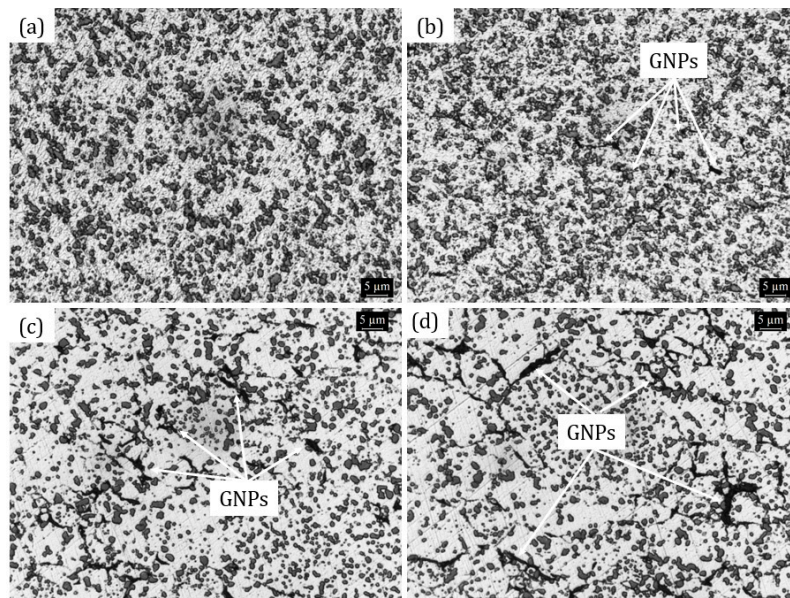

Figure 3. Light micrographs of (**a**) AlSi10Mg, (**b**) AlSi10Mg–0.5 wt.% GNPs, (**c**) AlSi10Mg–1 wt.% and (**d**) AlSi10Mg–2 wt.% GNPs after hot consolidation perpendicular to the compaction direction.
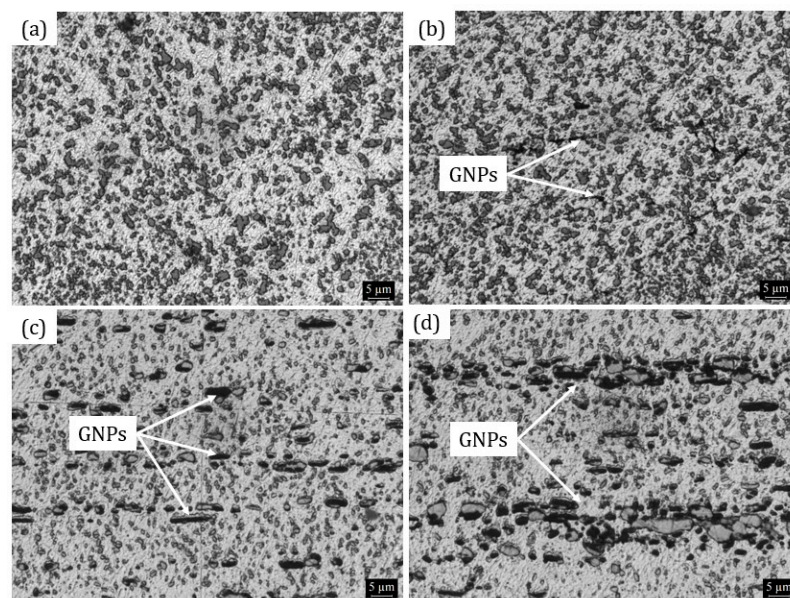

Figure 4. Light micrographs of (**a**) AlSi10Mg, (**b**) AlSi10Mg–0.5 wt.% GNPs, (**c**) AlSi10Mg–1 wt.% and (**d**) AlSi10Mg–2 wt.% GNPs after hot consolidation parallel to the compaction direction.

In general, it is reported that in the MMNCs reinforced by a reinforcing material, there are four types of interfacial bonding, including van der Waals attraction, mechanical bonding, reaction bonding and diffusion bonding [28]. Therefore, a more in-depth microstructural analysis demonstrates that the interfacial bonding between the matrix (AlSi10Mg) and reinforcement (GNPs) is a mechanical interlocking, which is the weakest type of interfacial bonding (Figure 5).
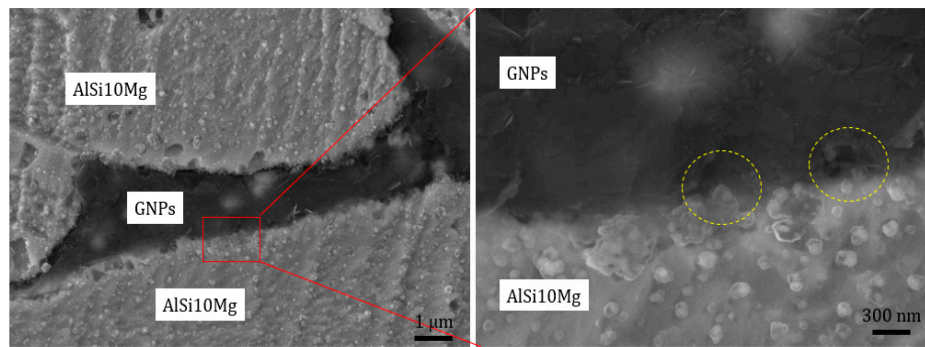
Figure 5. SEM micrographs of a representative interface between the AlSi10Mg/GNPs after hot consolidation.

3.2. Mechanical Properties Evaluation

The Vickers hardness and porosity content of pure AlSi10Mg and its composites is reported in Figure 6. It is evident that by the addition of GNPs, the Vickers hardness of nanocomposites increases up to 30% at low GNPs contents and then decreases at higher GNPs contents. The improvement of hardness can be explained by the presence of GNPs with high strength in such a way that they introduce a high constraint during indentation.
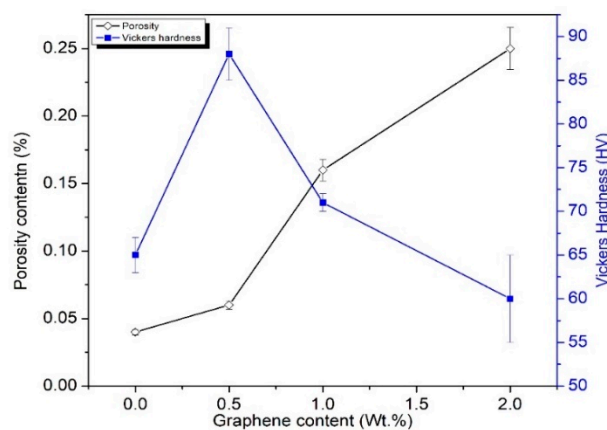

Figure 6. Porosity content and Vickers hardness variations as a function of graphene content.

The effect of porosity on the mechanical feature of the composites can be confirmed by comparing the hardness and the internal porosity fraction. It was found that the samples with the lowest internal porosity present the highest hardness. These results indicate that there is a threshold for the GNPs (0.5 wt.%). In fact, before that threshold, the strengthening mechanisms such as grain refinement and Orowan looping work efficiently, whereas, after that threshold, graphene agglomeration neutralizes the strengthening mechanisms and accordingly deteriorates the mechanical performance of the nanocomposites.

The variation of Yield Strength (YS), Ultimate Tensile Strength (UTS) and Failure Strain (FS%) of AlSi10Mg–xGNPs (x = 0, 0.5, 1, 2 wt.%) nanocomposites as a function of graphene content is shown in Figure 7. From a statistical point of view, these values are the average of numbers that are calculated according to engineering σ–ε curves of three repeated tests. From the graph above, we can see that the same trend of hardness with the GNPs content is also seen in the tensile properties. As can be seen in Figure 7, by the addition of 0.5 wt.% of GNPs, the UTS value of nanocomposite is gently increased, whereas additions exceeding 1 wt.% deteriorates the tensile characteristics. The deterioration of tensile properties leads to a decrease in the values of UTS and FS in comparison with that of AlSi10Mg. These findings are also in line with a previous work on the mechanical properties of AlSi10Mg-GNPs [29,30]. The mechanical features improvement of AlSi10Mg–0.5 wt.% GNPs can be related to the hindering of dislocation motion across the matrix/reinforcement interface by GNPs during the tensile loading

(Orowan looping) and grain refinement that was achieved through the addition of GNPs [21]. As a result of hindering the dislocations (Orowan looping), $\Delta\sigma_{\text{Orowan}}$, the yield strength of composites increased, which can be explained according to the following equation [31]:

$$\Delta\sigma_{\text{Orowan}} = \frac{0.13Gb}{d_{\text{P}}\left[\left(1/2f_{\text{v}}\right)^{1/3} - 1\right]} \ln\left(\frac{d_{\text{P}}}{2b}\right) \tag{1}$$
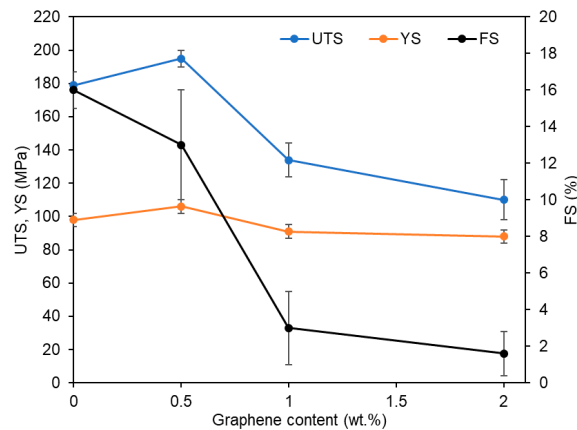

Figure 7. Yield strength, ultimate tensile strength and failure strain of AlSi10Mg/GNPs nanocomposites as a function of graphene content.

It is reported that by decreasing the space between the graphene nanoplatelets within the matrix (through a uniform dispersion), the strengthening effect by this mechanism increases.

Grain refinement is another strengthening mechanism that participates in the strengthening of the nanocomposite. In fact, this mechanism relies on the particle size and volume fraction on nanoparticles so that the grain size (d_{m}) decreases either by increasing the volume fraction of particles (V_{p}) or decreasing the particle size (d_{p}). As discussed earlier, in this work is also found that by increasing the GNPs content the grain sized decreases gradually. Grain refinement as a consequence of GNPs addition and accordingly strengthening of nanocomposite is reported in previous works [19,21,27].

Since the type of interfacial bonding between the GNPs and matrix is mechanical interlocking the load transfer and Coefficient of Thermal Expansion (CTE)-mismatch strengthening mechanisms are not effective in this nanocomposite, whereas Orowan looping and Hall-Petch strengthening are slightly effective at low GNPs contents. Figure 7 also shows that the slight strengthening at low GNPs content is achieved by sacrificing the failure strain. On the other hand, the Pi-Pi attractions between layers of graphene might consequence in a formation of a thick graphite particle so that could be explained the reduction of FS% in AlSi10Mg at the presence of 0.5 wt.% GNPs. In addition, the lower mechanical performance of the nanocomposites at high graphene contents is associated with the graphene agglomeration. Therefore, a negative defect is activated in the GNPs agglomerate, in addition to the poor interfacial bonding and preferred orientation of graphene concerning the tensile direction. Indeed, the presence of weak bonds between the graphene nanoplatelets, higher porosity content as a consequence of agglomeration and poor interfacial bonding between the matrix and reinforcement deteriorate the mechanical performance of the nanocomposites at higher GNPs content. Moreover, these defects can act as the stress concentrator and result in the deterioration of mechanical properties, as is clear in Figure 8d, where an apparent brittle fracture area surrounds a platelet. Each of these defects individually plays a key role in the final properties of nanocomposites. For instance, the interface bonding between reinforcement and matrix has a significant role in the load transfer from the matrix to reinforcement [32,33]. This finding is also reported in the literature about the MMNCs reinforced by GNPs [26]. The FESEM images of the fracture surface of the AlSi10Mg nanocomposites with different GNPs contents are shown after the tensile test at ambient temperature. In principle,

the failure mainly occurred in the AlSi10Mg and AlSi10Mg–0.5wt.% GNPs composites through the void coalescence cause to the ductility of AlSi10Mg alloy matrix. As can be seen, by increasing the GNPs content and decreasing the ductility, the fracture mode convert step by step from a ductile fracture mode to a brittle fracture mode. This change in the fracture more can be attributed to several issues, such as the formation of agglomerates and consequently higher porosity content and the poor interfacial bonding between AlSi10Mg and GNPs. In fact, a high content of GNPs in Al alloys causes the incrementing of the porosity content, which can act as a crack initiation source during the tensile loading as reported in previous researches [19].
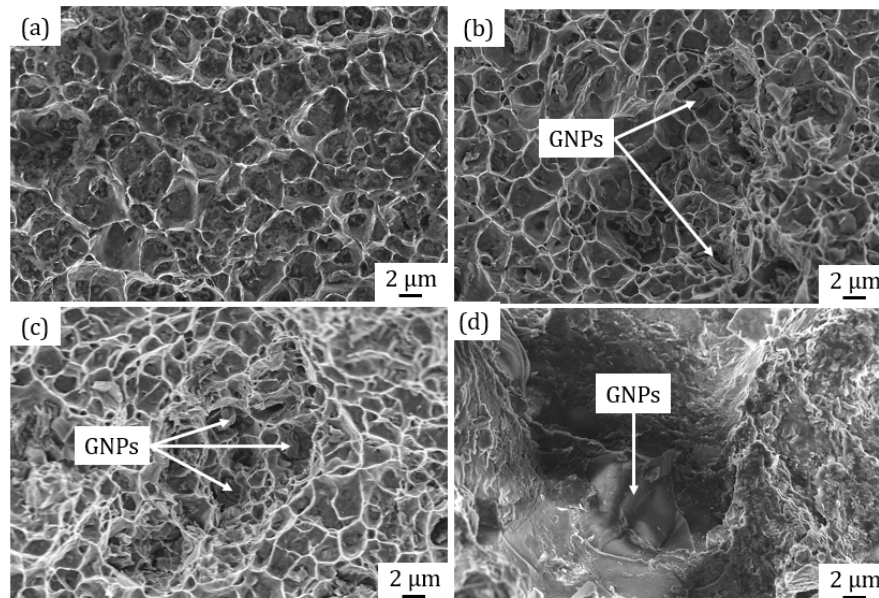

Figure 8. Fracture surface of (**a**) AlSi10Mg, (**b**) AlSi10Mg–0.5 wt.% GNPs, (**c**) AlSi10Mg–1 wt.% GNPs and (**d**) AlSi10Mg–2 wt.% GNPs after tensile test.

As discussed earlier, based on the inherent characteristics of GNPs, the week physical bonding between the layers of GNPs is much lower than strong chemical bonding between the atoms of the same layer that mentioned as the out-of-plane strength and in-plane strength, respectively. As clearly shown in Figure 8d, the poor interfacial bonding between the GNPs and matrix does not let the GNPs participate in the strengthening of the nanocomposites and the voids at their interface act as the crack initiation points and finally results in brittle failure. Moreover, from Figure 8a–c, it is possible to see that the size of the dimple reduced significantly, which is as a consequence of grain refinement and strengthening the effect of GNPs.

3.3. Thermal Properties

Superior properties of GNPs make this material a proper candidate to be used in MMNCs to improve their Thermo-physical properties and accordingly broaden their applications in electronic packaging industries. Therefore, in this work to assess the effect of GNPs on the thermal conductivity of AlSi10Mg/GNPs nanocomposites at high temperatures, their thermal diffusivity was measured via laser flash method, and then their thermal conductivity was calculated. Figure 9 shows the thermal conductivity of AlSi10Mg and its nanocomposites up to 400 °C. As can be seen in this figure, the thermal conductivity of AlSi10Mg–0.5% GNPs slightly increases with respect to the AlSi10Mg alloy, whereas the thermal conductivity of the nanocomposites with higher graphene contents (≥1 wt.%) is deteriorated. This significant difference in the thermal conductivities is directly attributed to the graphene content. Indeed, as revealed earlier in Figure 3, by increasing the quantity of GNPs, the number of agglomerates increases markedly, and higher porosity content is the first important

consequence that destroys the thermal conductivity of the nanocomposite. Moreover, as is shown in Figure 5, there is no strong interfacial bonding between the matrix and reinforcement and this weak interfacial bonding could result in lower thermal conductivities. This hypothesis can be confirmed by the correlation between the porosity content of the nanocomposite with 1% and 2%GNPs and their thermal conductivities. This means that in comparison with the AlSi10Mg–1%GNPs with 0.15% porosity content, AlSi10Mg–2%GNPs had much lower thermal conductivity.
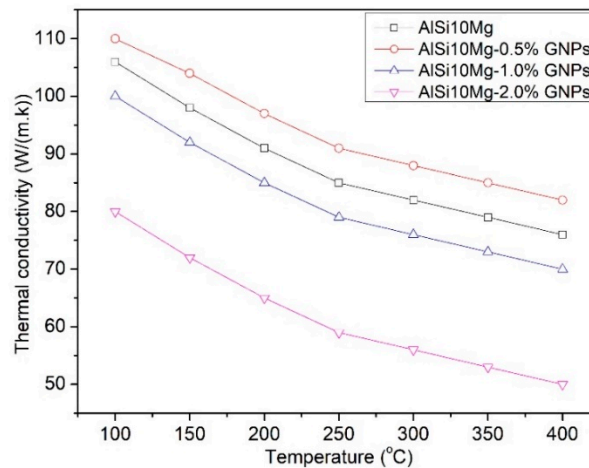

Figure 9. Thermal conductivity of AlSi10Mg–*x* wt.% GNPs (*x* = 0, 0.5, 1.0 and 2) after hot consolidation.

The interfacial thermal resistance of the AlSi10Mg/GNPs can be estimated via the acoustic mismatch model (AMM) model [34]:

$$h = \frac{1}{2}\rho_{in}C_{in}\frac{\rho_{in}\rho_{tran}\vartheta_{in}^4}{\vartheta_{tran}(\rho_{in}\vartheta_{in} + \rho_{tran}\vartheta_{tran})^2} \tag{2}$$

where C, ρ and ϑ are the specific heat, density and phonon velocity, respectively. Terms of "in" and "tran" as subscripts are referring to the incident and transmission sides of the phonon, respectively. Since the transversal waves contribute to heat transfer, their velocities were taken into account. By using the datasheet of starting materials and also data presented in the previous works [35] in Equation (2), the interfacial resistance between the matrix and reinforcement is $h = 5.3 \times 10^7$ W·m^{-2}·K^{-1}, which is slightly higher than the resistance that is reported for Al/GNPs (5×10^7 W·m^{-2}·K^{-1} [36,37]).

4. Conclusions

In this research, wet mixing method and hot consolidation (600 °C) were used for synthesizing of AlSi10Mg–*x*GNPs (*x* = 0, 0.5, 1 and 2 wt.%) nanocomposites. Based on the results, the following conclusions can be drawn:

- Wet mixing method has a great potential to be used as a mixing method to homogeneously disperse a low quantity of GNPs within the AlSi10Mg matrix.
- In the mixing of AlSi10Mg/GNPs, there is a critical threshold for the quantity of GNPs that should be considered, in such a way that after this critical quantity GNPs start to for agglomerates and deteriorate the final properties of nanocomposites.
- By increasing the quantity of GNPs, the residual porosity content increases dramatically.
- Grain refinement is one of the significant effects of graphene addition on the microstructure of AlSi10Mg/GNPs nanocomposites and plays a key role in the strengthening of the nanocomposites through the Hall-Petch strengthening effect.
- In-depth microstructural investigations revealed that the interfacial bonding between AlSi10Mg and GNPs is one of the weakest types interfaces, which is called mechanical interlocking.

- The effect of GNPs addition on mechanical characteristics (UTS, YS, FS and hardness) of AlSi10Mg was investigated. It was found that the AlSi10Mg nanocomposites with 0.5 wt.% GNPs presented the highest hardness and UTS, which could be associated with the grain refinement as the primary strengthening mechanism.

- Surprisingly, AlSi10Mg–1 and 2% GNPs nanocomposites presented lower mechanical properties with respect to the un-reinforced AlSi10Mg alloy, which might be as a consequence of GNP agglomeration and higher porosity content.

- The same trend of mechanical properties is also achieved in the thermal conductivity of the nanocomposites in which, at the low quantity of GNPs, the thermal conductivity of the nanocomposite increased slightly, whereas at higher GNPs contents, their thermal conductivities deteriorated.

- The interfacial thermal resistance of the AlSi10Mg/GNPs was estimated via the acoustic mismatch model (AMM) model, and the outcome shows that the interfacial resistance between AlSi10Mg/GNPs is slightly higher than Al/GNPs.

Author Contributions: In this work, S.K.M. and M.D. conceived and designed the experiments and thereafter performed the experiments. M.D. analyzed the data. S.K.M. and M.D. wrote the paper and A.S. supervised the work and revised the paper.

Conflicts of Interest: The authors declare no conflict of interest.

References

1. Geim, A.K.; Novoselov, K.S. The rise of graphene. *Nat. Mater.* **2007**, *6*, 183–191. [CrossRef] [PubMed]
2. Balandin, A.A.; Ghosh, S.; Bao, W.; Calizo, I.; Teweldebrhan, D.; Miao, F.; Lau, C.N. Superior thermal conductivity of single-layer graphene. *Nano Lett.* **2008**, *8*, 902–907. [CrossRef] [PubMed]
3. Saboori, A.; Moheimani, S.K.; Pavese, M.; Badini, C.; Fino, P. New nanocomposite materials with improved mechanical strength and tailored coefficient of thermal expansion for electro-packaging applications. *Metals* **2017**, *7*, 536. [CrossRef]
4. Faccio, R.; Denis, P.A.; Pardo, H.; Goyenola, C.; Álvaro, W. Mechanical properties of graphene nanoribbons. *J. Phys. Condens. Matter.* **2009**, *21*, 285–304. [CrossRef] [PubMed]
5. Stankovich, S.; Dikin, D.A.; Dommett, G.H.B.; Kohlhaas, K.M.; Zimney, E.J.; Stach, E.A.; Piner, R.D.; Nguyen, S.T.; Ruoff, R.S. Graphene-based composite materials. *Nature* **2006**, *442*, 282–286. [CrossRef] [PubMed]
6. Saboori, A.; Pavese, M.; Badini, C.; Fino, P. A novel approach to enhance the mechanical strength and electrical and thermal conductivity of Cu-GNP nanocomposites. *Metall. Mater. Trans. A Phys. Metall. Mater. Sci.* **2018**, *49*, 333–345. [CrossRef]
7. Zhang, Y.Y.; Wang, C.M.; Cheng, Y.; Xiang, Y. Mechanical properties of bilayer graphene sheets coupled by sp3 bonding. *Carbon* **2011**, *49*, 4511–4517. [CrossRef]
8. Hong, N.; Zhan, J.; Wang, X.; Stec, A.A.; Hull, T.R.; Ge, H.; Xing, W.; Song, L.; Hu, Y. Enhanced mechanical, thermal and flame retardant properties by combining graphene nanosheets and metal hydroxide nanorods for Acrylonitrile–Butadiene–Styrene copolymer composite. *Compos. Part. A Appl. Sci. Manuf.* **2014**, *64*, 203–210. [CrossRef]
9. Hu, K.; Kulkarni, D.D.; Choi, I.; Tsukruk, V.V. Graphene-polymer nanocomposites for structural and functional applications. *Prog. Polym. Sci.* **2014**, *39*, 1934–1972. [CrossRef]
10. Wang, K.; Wang, Y.; Fan, Z.; Yan, J.; Wei, T. Preparation of graphene nanosheet/alumina composites by spark plasma sintering. *Mater. Res. Bull.* **2011**, *46*, 315–318. [CrossRef]
11. Walker, L.S.; Marotto, V.R.; Rafiee, M.A.; Koratkar, N.; Corral, E.L. Toughening in graphene ceramic composites. *ACS Nano* **2011**, *5*, 3182–3190. [CrossRef] [PubMed]
12. Kim, W.J.; Lee, T.J.; Han, S.H. Multi-layer graphene/copper composites: Preparation using high-ratio differential speed rolling, microstructure and mechanical properties. *Carbon* **2014**, *69*, 55–65. [CrossRef]
13. Chen, L.; Zhao, Y.; Hou, H.; Zhang, T.; Liang, J.; Li, M.; Li, J. Development of AZ91D magnesium alloy-graphene nanoplatelets composites using thixomolding process. *J. Alloys Compd.* **2019**, *778*, 359–374. [CrossRef]

14. Wang, H.; Zhang, K.; Zhang, M. Fabrication and properties of Ni-modified graphene nanosheets reinforced Sn-Ag-Cu composite solder. *J. Alloys Compd.* **2019**, *781*, 761–772. [CrossRef]

15. Jagannadham, K. Volume fraction of graphene platelets in copper-graphene composites. *Met. Mater. Trans. A* **2013**, *44*, 552–559. [CrossRef]

16. Saboori, A.; Pavese, M.; Badini, C.; Fino, P. A novel Cu-GNPs nanocomposite with improved thermal and mechanical properties. *Acta Met. Sin. English Lett.* **2018**, *31*, 148–152. [CrossRef]

17. Saboori, A.; Pavese, M.; Badini, C.; Fino, P. Effect of sample preparation on the microstructural evaluation of Al-GNPs nanocomposites. *Met. Microstruct. Anal.* **2017**, *6*, 619–622. [CrossRef]

18. Shao, P.; Yang, W.; Zhang, Q.; Meng, Q.; Tan, X.; Xiu, Z.; Qiao, J.; Yu, Z.; Wu, G. Microstructure and tensile properties of 5083 Al matrix composites reinforced with graphene oxide and graphene nanoplates prepared by pressure infiltration method. *Compos. Part A Appl. Sci. Manuf.* **2018**, *109*, 151–162. [CrossRef]

19. Rashad, M.; Pan, F.; Tang, A.; Asif, M. Effect of graphene nanoplatelets addition on mechanical properties of pure aluminum using a semi-powder method. *Prog. Nat. Sci. Mater. Int.* **2014**, *24*, 101–108. [CrossRef]

20. Wang, J.; Li, Z.; Fan, G.; Pan, H.; Chen, Z.; Zhang, D. Reinforcement with graphene nanosheets in aluminum matrix composites. *Scr. Mater.* **2012**, *66*, 594–597. [CrossRef]

21. Saboori, A.; Pavese, M.; Badini, C.; Fino, P. Microstructure and thermal conductivity of Al-graphene composites fabricated by powder metallurgy and hot rolling techniques. *Acta Metall. Sin. English Lett.* **2017**, *30*, 675–687. [CrossRef]

22. Saboori, A.; Novara, C.; Pavese, M.; Badini, C.; Giorgis, F.; Fino, P. An investigation on the sinterability and the compaction behavior of aluminum/graphene nanoplatelets (GNPs) prepared by powder metallurgy. *J. Mater. Eng. Perform.* **2017**, *26*, 993–999. [CrossRef]

23. Rashad, M.; Pan, F.; Hu, H.; Asif, M.; Hussain, S.; She, J. Enhanced tensile properties of magnesium composites reinforced with graphene nanoplatelets. *Mater. Sci. Eng. A* **2015**, *630*, 36–44. [CrossRef]

24. Bartolucci, S.F.; Paras, J.; Rafiee, M.A.; Rafiee, J.; Lee, S.; Kapoor, D.; Koratkar, N. Graphene–aluminum nanocomposites. *Mater. Sci. Eng. A* **2011**, *528*, 7933–7937. [CrossRef]

25. Rashad, M.; Pan, F.; Asif, M.; Tang, A. Powder metallurgy of Mg–1%Al–1%Sn alloy reinforced with low content of graphene nanoplatelets (GNPs). *J. Ind. Eng. Chem.* **2014**, *20*, 4250–4255. [CrossRef]

26. Saboori, A.; Dadkhah, M.; Fino, P.; Pavese, M. An overview of metal matrix nanocomposites reinforced with graphene nanoplatelets; Mechanical, electrical and thermophysical properties. *Metals* **2018**, *8*, 423. [CrossRef]

27. Saboori, A.; Moheimani, S.K.; Dadkhah, M.; Pavese, M.; Badini, C.; Fino, P. An overview of key challenges in the fabrication of metal matrix nanocomposites reinforced by graphene nanoplatelets. *Metals* **2018**, *8*, 172. [CrossRef]

28. Chu, K.; Liu, Z.; Jia, C.; Chen, H.; Liang, X.; Gao, W. Thermal conductivity of SPS consolidated Cu/diamond composites with Cr-coated diamond particles. *J. Alloy. Compd.* **2010**, *490*, 453–458. [CrossRef]

29. Kandemir, S. Effect of graphene nanoplatelets reinforcement on the microstructure and mechanical properties of AlSi10Mg alloy. *GU J. Sci. Part C* **2018**, *6*, 177–187.

30. Saboori, A.; Casati, R.; Zanatta, A.; Pavese, M.; Badini, C.; Vedani, M. Effect of Graphene nanoplatelets on microstructure and mechanical properties of AlSi10Mg nanocomposites produced by hot extrusion. *Powder Metall. Met. Ceram.* **2018**, *56*, 647–655. [CrossRef]

31. Ferguson, J.B.; Sheykh-Jaberi, F.; Kim, C.-S.; Rohatgi, P.K.; Cho, K. On the strength and strain to failure in particle-reinforced magnesium metal-matrix nanocomposites (Mg MMNCs). *Mater. Sci. Eng. A* **2012**, *558*, 193–204. [CrossRef]

32. Luster, J.W.; Thumann, M.; Baumann, R. Mechanical properties of aluminium alloy 6061–Al_2O_3 composites. *Mater. Sci. Technol.* **1993**, *9*, 853–862. [CrossRef]

33. Aikin, R.M.; Christodoulou, L. The role of equiaxed particles on the yield stress of composites. *Scr. Metall. Mater.* **1991**, *25*, 9–14. [CrossRef]

34. Swartz, E.T.; Pohl, R.O. Thermal boundary resistance. *Rev. Mod. Phys.* **1989**, *61*, 605. [CrossRef]

35. Dewar, B.; Nicholas, M.; Scott, P.M. The solid phase bonding of copper, nickel and some of their alloys to diamonds. *J. Mater. Sci.* **1976**, *11*, 1083–1090. [CrossRef]

36. Xue, C.; Bai, H.; Tao, P.F.; Wang, J.W.; Jiang, N.; Wang, S.L. Thermal conductivity and mechanical properties of flake graphite/Al composite with a SiC nano-layer on graphite surface. *Mater. Des.* **2016**, *108*, 250–258. [CrossRef]

37. Schmidt, A.J.; Collins, K.C.; Minnich, A.J.; Chen, G. Thermal conductance and phonon transmissivity of metal-graphite interfaces. *J. Appl. Phys.* **2010**, *107*, 104–107. [CrossRef]